PNAS RESEARCH ARTICLE | BIOPHYSICS AND COMPUTATIONAL BIOLOGY

The β2-adrenergic receptor associates with CXCR4 multimers in human cancer cells

Junyi Liang[a,1], Mohamed Seghiri[a,b], Pradeep Kumar Singh[a,b], Hyeon Gyu Seo[c], Ji Yeong Lee[c], Yoonjung Jo[c], Yong Bhum Song[d], Chulo Park[d], Piotr Zalicki[c], Jae-Yeon Jeong[c], Won-Ki Huh[d,e], Niña G. Caculitan[c,2], and Adam W. Smith[a,b,2]

Edited by Robert Lefkowitz, HHMI, Durham, NC; received March 27, 2023; accepted February 12, 2024

While the existence and functional role of class C G-protein-coupled receptors (GPCR) dimers is well established, there is still a lack of consensus regarding class A and B GPCR multimerization. This lack of consensus is largely due to the inherent challenges of demonstrating the presence of multimeric receptor complexes in a physiologically relevant cellular context. The C-X-C motif chemokine receptor 4 (CXCR4) is a class A GPCR that is a promising target of anticancer therapy. Here, we investigated the potential of CXCR4 to form multimeric complexes with other GPCRs and characterized the relative size of the complexes in a live-cell environment. Using a bimolecular fluorescence complementation (BiFC) assay, we identified the β2 adrenergic receptor (β2AR) as an interaction partner. To investigate the molecular scale details of CXCR4-β2AR interactions, we used a time-resolved fluorescence spectroscopy method called pulsed-interleaved excitation fluorescence cross-correlation spectroscopy (PIE-FCCS). PIE-FCCS can resolve membrane protein density, diffusion, and multimerization state in live cells at physiological expression levels. We probed CXCR4 and β2AR homo- and heteromultimerization in model cell lines and found that CXCR4 assembles into multimeric complexes larger than dimers in MDA-MB-231 human breast cancer cells and in HCC4006 human lung cancer cells. We also found that β2AR associates with CXCR4 multimers in MDA-MB-231 and HCC4006 cells to a higher degree than in COS-7 and CHO cells and in a ligand-dependent manner. These results suggest that CXCR4-β2AR heteromers are present in human cancer cells and that GPCR multimerization is significantly affected by the plasma membrane environment.

G-protein-coupled receptors | fluorescence spectroscopy | membrane protein interactions

Significance

Both CXCR4 and β2AR are expressed in cancer cells and play active roles in oncogenesis. We use a time-resolved fluorescence approach to quantify CXCR4 and β2AR interactions in live cells at physiological conditions. The results are consistent with a model in which CXCR4 forms clusters of several receptors (i.e., multimers) in two cancer cell lines and that β2AR associates with the CXCR4 multimers. These results may aid in the development of pharmaceutical approaches to treat CXCR4-positive cancers, especially using combination therapies or bivalent compounds. The experimental approach described here could be applicable to investigations of other membrane protein interactions in their living cellular environments.

Accounting for over 30% of FDA-approved drugs (1), G-protein-coupled receptors (GPCRs) are one of the most heavily investigated protein families in drug development. Currently, the full complexity of GPCR signaling is still not well understood, especially with respect to the propensity of GPCRs to form homomeric and heteromeric complexes with biochemical properties distinct from their individual components (2, 3). While the existence and functional role of class C GPCR dimers is well established, there is still a lack of consensus regarding the existence and functional relevance of class A and B GPCR multimerization. This is due in part to the inherent challenges of demonstrating the presence of those receptor complexes in physiologically relevant cellular context. The growth and improvement of quantitative, live-cell assays like single-molecule tracking (SMT), Förster resonance energy transfer (FRET), and fluorescence correlation spectroscopy (FCS) have begun to clarify earlier controversies on the existence of these oligomeric complexes. For example, SMT has been used to quantify the density-dependent homodimerization of the C-X-C motif chemokine receptor 4 (CXCR4), a class A GPCR (4). Indeed, the biology of CXCR4, a chemokine receptor that regulates cell proliferation, hematopoiesis, tissue regeneration, and tumorigenesis, has been studied quite heavily. CXCR4 is overexpressed in 23 cancers and has been investigated in clinical trials for heme malignancies and solid tumors, such as breast and lung cancers (5–10).

In recent years, many studies have investigated CXCR4 oligomerization (4, 11–15). Like other chemokine receptors, CXCR4 can form homodimers (14), trimers (16), and higher-order complexes (17). CXCR4 was also shown to heterodimerize with various chemokine receptors including CCR2 (11), CCR5 (18, 19), CXCR3 (20), CXCR7 (or ACKR3) (21), as well as with other class A GPCRs such as the cannabinoid receptor 2 (CB2R) (22). The physical interactions between receptors within multimeric complexes are thought to have functional relevance in the activation of signaling pathways downstream of GPCRs (23, 24).

The toolset for the characterization of multimerization has evolved from bulk static measurements, such as immunoprecipitation methods and fluorescence/bioluminescence resonance energy transfer (FRET/BRET) based assays, to lower throughput but more

Author contributions: J.L., M.S., H.G.S., J.Y.L., Y.S., J.-Y.J., W.-K.H., N.G.C., and A.W.S. designed research; J.L., M.S., P.K.S., H.G.S., J.Y.L., Y.J., Y.B.S., C.P., and P.Z. performed research; J.L., M.S., P.K.S., H.G.S., J.Y.L., Y.J., Y.B.S., C.P., and A.W.S. analyzed data; and J.L., M.S., J.-Y.J., W.-K.H., N.G.C., and A.W.S. wrote the paper.

Competing interest statement: Several authors are employees of GPCR Therapeutics Inc., the sponsor of this research.

This article is a PNAS Direct Submission.

[1]Present address: Genomic Medicine Institute, Cleveland Clinic, Cleveland, OH 44195.

[2]To whom correspondence may be addressed. Email: nina.caculitan@gpcrtx.com or aw.smith@ttu.edu.

This article contains supporting information online at https://www.pnas.org/lookup/suppl/doi:10.1073/pnas.2304897121/-/DCSupplemental.

Published March 28, 2024.

precise methods that can detect individual multimers and their dynamic behavior on the living cell surface. FRET or BRET assays are widely used to study protein–protein interactions in living cells and are scalable for screening purposes. However, they cannot precisely quantify receptor density, diffusion, and multimeric state parameters which are crucially important for understanding GPCR complexes in their native environment (25, 26). FRET or BRET assays can also be sensitive to false positives due to random receptor colocalization and transient collisions that often occur at higher densities (27).

For more accurate measurements of protein diffusion and interactions, higher-resolution microscopy-based methods, such as SMT, FCS, and fluorescence cross-correlation spectroscopy (FCCS) can be employed. These methods enable detailed characterization of a receptor's density, diffusion, and oligomeric state. A time-correlated single-photon counting version of FCCS called pulsed interleaved excitation (PIE)-FCCS offers the additional advantage of directly removing cross talk between the two overlapping fluorescence spectra (28). PIE-FCCS was first used in live cells to elucidate the nature of EGFR dimerization on the cell membrane (29). The use of known calibration standards such as membrane proteins that are known to be monomers, dimers, and multimers was critical for accurate enumeration of the composition of protein multimers (30). PIE-FCCS measurements of membrane proteins with an inducible dimerization motif (FKBP) were used to develop and test a quantitative model of membrane protein multimerization (31). This approach was used recently to resolve the dimerization state of several representative GPCRs for direct comparison to single-molecule FRET (32). PIE-FCCS allows for the measurement of receptor mobility and dimerization at physiologically relevant densities and sampling rates (33). PIE-FCCS is sensitive to stable molecular interactions at concentrations as low as 10 and up to 5,000 molecules/μm^2 (33). Notably, SMT requires very low expression levels (below 1 molecule/μm^2), well below the expression levels of chemokine receptors in cancer cells (4). Additionally, PIE-FCCS acts as a spatiotemporal filter in that it effectively removes large stationary aggregates and interior organelles from the data analysis. This sensitivity to freely diffusing proteins helps to eliminate some of the artifacts that may result in false-positive dimerization using bulk fluorescence techniques such as BRET and FRET methods (34, 35).

In this study, we first employed an agnostic approach to CXCR4 heteromer pair detection with bimolecular fluorescence complementation (BiFC) and found CXCR4-β2AR as a significant interaction pair. The β2-adrenergic receptor (β2AR) is a member of the class A GPCR family. Recent research has demonstrated a connection between β2ARs and several cancer-related phenotypes, including cell proliferation (36), apoptosis resistance (37), metastasis (38), and tumor growth (39). On the other hand, current literature has yet to reach a consensus about the prevalence of β2AR homodimerization (35, 40–42). CXCR4-β2AR heterodimerization in living cells has been reported in the context of myocardial biology using a BRET-based assay on human embryonic kidney (HEK) cells (41). However, this earlier work did not characterize the physical properties of the receptor homomers and the CXCR4- β2AR heteromers nor the dependence on the cellular context. Here, we investigate oligomerization in cancer cells and the impact on oncogenic behavior.

In order to validate and characterize the CXCR4-β2AR heteromers we detected in our BiFC assay, we utilized PIE-FCCS to probe receptor multimerization in several cell lines: COS-7, Chinese hamster ovary (CHO) cells, MDA-MB-231, and HCC4006. COS-7 is a simian fibroblast while CHO cells, along with HEK cells, are the most commonly used cell lines for SMT and FCS/FCCS studies. MDA-MB-231 and HCC4006 are human breast and lung cancer cell lines, respectively. We found that while CXCR4 forms mostly homodimers in COS-7 and CHO cells, it self-associates into small multimers of three to four CXCR4 molecules in MDA-MB-231 and HCC4006 cells. Interestingly, whereas the size of the CXCR4 homomultimers is cell line–dependent, β2AR homomultimer size is not. Finally, we found that β2AR monomers and dimers associate with CXCR4 multimers to form large protein clusters. This characterization of CXCR4-β2AR multimers in live cancer cells highlights the importance of cellular context as well as the interplay between receptor structure, agonism/antagonism, and oligomerization state on downstream signaling and behavior.

Results

BiFC Reveals CXCR4- β2AR As GPCR Heteromers Pair. CXCR4-GPCRx heteromers were identified using a BiFC assay (Fig. 1*A*). First, a library of recombinant adenoviruses encoding 143 GPCRs fused with N-terminal fragments of yellow fluorescent protein, Venus (VN), and 147 GPCRs fused with C-terminal fragment of Venus (VC) was made as described in Song et al. (43). Cells that expressed CXCR4-VN and GPCRx-VC or CXCR4-VC and GPCRx-VN would become fluorescent only when the receptors with complementary VN and VC regions are in close proximity (44). One notable feature of the BiFC assay is the strong binding affinity between VN and VC, resulting in self-assembly of the Venus protein. Although this feature enables the detection of weak or transient interactions among diverse protein partners, it could potentially generate false-positive interaction data. Hence, it is crucial to employ appropriate controls. When CXCR4-VN was coexpressed with HA-VC or μ-opioid receptor (μOR)-VC, no BiFC signal was observed (Fig. 1*B*). This was used as the negative control. In contrast, when CXCR4-VN was coexpressed with CXCR4-VC, the BiFC signal was observed in the plasma membrane and in the cytoplasm. This was used as the positive control. Strong BiFC signal was observed in the plasma membrane and in the cytoplasm when CXCR4-VN was cotransfected with ADRB2-VC (Fig. 1*B*). Cells that showed BiFC fluorescence signal higher than the background level were counted as BiFC positive cells, and the BiFC score was calculated. The BiFC screening approach yielded the following GPCRs as interactors of CXCR4: ADCYAP1R1, ADORA2B, ADORA3, β2AR (ADRB2),

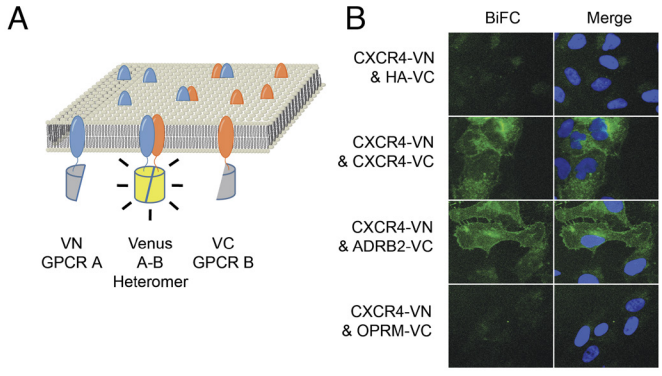

Fig. 1. (*A*) Schematic drawing of the bimolecular fluorescence complementation (BiFC) assay. GPCR A is fused with the N-terminal fragment of yellow fluorescent protein (YFP) Venus (VN), and GPCR B is fused with the C-terminal fragment of Venus (VC). When GPCR A and B form a heteromer, the complementary VN and VC are close enough to form a functional Venus. (*B*) Fluorescence images showing the degree of fluorescence, which is indicative of complementation.

APLNR, C5AR1, CALCR, CCR5, CHRM1, GALR1, EDNRB, HRH1, LPAR1, MLNR, NTSR1, PTGER2, PTGER3, SSTR2, and TACR3 (45).

CXCR4 Is a Homomultimer in MDA-MB-231 and HCC4006 Human Cancer Cell Lines. We further investigated the CXCR4-β2AR heteromer using a time-resolved fluorescence method, PIE-FCCS, which allowed us to probe molecular interactions in live cells (Fig. 2*A*). First, we determined the degree of homomultimerization of CXCR4, beginning with COS-7 and MDA-MB-231 cell lines. CXCR4 was expressed as two constructs with spectrally distinct fluorescent protein fusions (CXCR4-AcGFP1 and CXCR4-mCherry). The fluorescence signal was collected from a single diffraction-limited area focused on the plasma membrane at the cell periphery, and the data were analyzed to produce auto- and cross-correlation functions (ACF and CCF). The amplitudes of the correlation functions were used to calculate the expression levels of the proteins and the relative cross-correlation (f_c), which is a measure of correlated diffusion and scales with the degree of interaction between the two constructs (Fig. 2*B*). To further characterize the multimerization state, we also calculated the diffusion coefficients of the proteins using the decay time of the ACFs. Diffusion coefficients are inversely related to the degree of receptor oligomerization. By comparison to monomer, dimer, and multimer membrane protein controls (31, 32), we could determine the oligomerization state of the protein (Fig. 2*D*). Precise measurements of f_c values and diffusion coefficients have been calibrated against defined multimerization standards for a number of transmembrane proteins in live cell membranes, including GPCRs. Therefore, the f_c values and diffusion coefficients provide a reliable and validated measure of membrane protein multimerization.

The expression levels of each exogenous receptor population were quantified from the PIE-FCCS data: 1,572 ± 452 molecules/μm^2 in COS-7 cells compared to 983 ± 511 molecules/μm^2 in MDA-MB-231 (*SI Appendix*, Table S1). Three different membrane-anchored FKBP constructs that can be chemically induced to oligomerize were used as dimer (1×FKBP), mixed dimer and multimer (2×FKBP), and multimer (3×FKBP) controls (Fig. 2*G*), as described previously (31). The median f_c value for the 1×FPKBP is f_c= 0.11, for the 2×FPKBP is f_c= 0.16, and for the 3×FKBP is f_c= 0.28 (31). The distribution of f_c values for CXCR4 had a median value of 0.18 (mean f_c = 0.22±0.17) in COS-7 cells, consistent with simple dimerization. In MDA-MB-231 cells, the distribution of f_c values was nearly twice as high (median f_c = 0.31, mean f_c = 0.39 ± 0.20, Fig. 2*D* and *SI Appendix*, Table S1) indicating the formation of higher-order oligomers. The average diffusion coefficient of CXCR4 was 0.21 ± 0.08 μm^2 s^{-1} in COS-7 cells compared to 0.14 ± 0.07 μm^2 s^{-1} in MDA-MB-231 (Fig. 2*E* and *SI Appendix*, Table S1). The diffusion coefficients and f_c values were consistent with a larger CXCR4 complex in MDA-MB-231 cells compared to simple dimerization in COS-7 cells (Fig. 2*F*). From these results, we conclude that CXCR4 is primarily a dimer in COS-7 cells, while in MDA-MB-231 cells at similarly high expression levels, CXCR4 is a multimer (oligomers on the order of trimers and tetramers). We repeated these experiments in CHO cells, a common cell line for live cell biophysical studies and previously

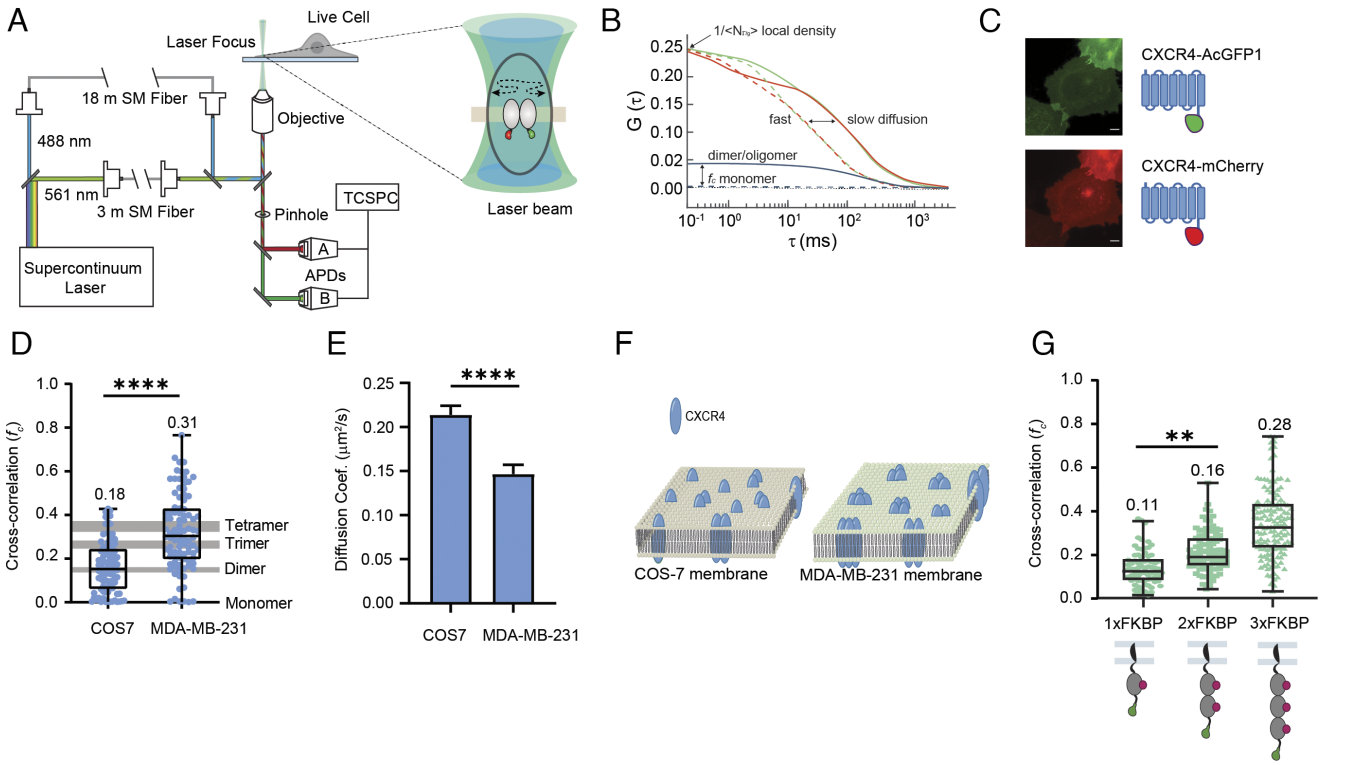

Fig. 2. Larger homomultimers of CXCR4 are observed in MDA-MB-231 cancer cells but not in COS-7 cells. (*A*) Schematic diagram of the PIE-FCCS setup (*B*) Illustrative examples of fluorescence intensity auto- and cross-correlation functions obtained from PIE-FCCS. (*C*) Representative epifluorescence images of COS7 cells expressing CXCR4 fused to AcGFP1 (*Top Left* image) and mCherry (*Bottom Left* image) at the C terminal and their schematic cartoons (*Right*). (Scale bars, 10 μm.) (*D*) Summary of single-cell cross-correlation values (f_c) for CXCR4 in COS-7 and MDA-MB-231 cells. The distribution of single-cell f_c values is plotted as well as the box and whisker plots. (*E*) Average diffusion coefficient of CXCR4 dimers in COS-7 and MDA-MB-231 cells. Error bars are ± the SD. (*F*) Schematic showing the formation of CXCR4 homomultimers in the COS-7 and MDA-MB-231 membranes. (*G*) Fractional correlation values of FKBP controls obtained in COS-7 cells using PIE-FCCS (31). Results show FKBP constructs after treatment with the ligand (AP20187) which stimulates oligomerization of the FKBP proteins. Each dot indicates the average value of five acquisitions per cell for 10 s. Data are shown as a box-and-whiskers plot, with the box representing the 25th to 75th percentile and the whiskers representing the highest and lowest values and the line inside the box representing the median value. For (*D*), (*E*), and (*G*), a paired *t* test was performed to obtain *P* values where ****P < 0.01, *P < 0.05, and ns > 0.5.

used in a CXCR4 homomultimerization study. We found a modest degree of cross-correlation similar to COS-7 cells (*SI Appendix*, Fig. S2). We also repeated the measurements in HCC4006 cells, a human lung cancer line in which the endogenous expression of CXCR4 and β2AR is low. We observed larger cross-correlation values compared to COS-7 and CHO, consistent with multimerization beyond simple dimerization (*SI Appendix*, Fig. S2).

β2AR Is a Weak Dimer in All Cell Lines Tested. We next set out to measure homo-oligomerization of β2AR with PIE-FCCS. We transiently coexpressed β2AR-AcGFP1 and β2AR-mCherry (Fig. 3*A*) in each cell line at a density of 878±365 molecules/μm^2 in COS-7 cells and 932 ± 602 molecules/μm^2 in MDA-MB-231 cells. (*SI Appendix*, Table S2). β2AR exhibited a modest degree of cross-correlation in COS-7 and MDA-MB-231 cells (Fig. 3*B*). The measured values of f_c = 0.13 ± 0.11 (median f_c = 0.09) in COS-7 cells and f_c = 0.11 ± 0.14 (median f_c = 0.07) in MDA-MB-231 (Fig. 3*C* and *SI Appendix*, Table S2) indicate that similar levels of β2AR homodimerization exist in both COS-7 and MDA-MB-231 cells. We also carried out similar experiments in CHO and HCC4006 cells, for which a modest degree of cross-correlation was also observed (median f_c = 0.02 for CHO and 0.07 for HCC4006, *SI Appendix*, Fig. S2 and Table S2). There was no statistically significant difference between the mobilities of β2AR in COS-7 cells (0.24 ± 0.09 μm^2 s^{-1}) compared to MDA-MB-231 cells (0.20 ± 0.19 μm^2 s^{-1}) (Fig. 3*D* and *SI Appendix*, Table S2), also supporting the conclusion that they are in the same monomer/dimer state in both cell lines.

CXCR4 and β2AR Assemble into Cell Line–Dependent Heterodimers. To ensure that the endogenous receptors did not interfere with the PIE-FCCS measurements, we generated a stable CXCR4/ β2AR double knockout (DKO) MDA-MB-231 mutants using CRISPR/Cas9. Orthogonal detection of protein expression via flow cytometry confirmed that both CXCR4 and β2AR genes were knocked out with no surface expression of either protein (*SI Appendix*, Fig. S1*A*). For comparison, we transiently transfected DKO MDA-MB-231 with CXCR4-AcGFP1 and β2AR-mCherry plasmids at the same levels as for the PIE-FCCS experiments and observed a significant increase in surface expression by flow cytometry (*SI Appendix*, Fig. S1*B*). From the PIE-FCCS experiments, we quantified the expression levels of CXCR4 and β2AR in measured cells to be at a total density of 1,123 ± 885 molecules/μm^2 and 1,686 ± 325 molecules/μm^2 in both COS-7 and DKO MDA-MB-231 cells, respectively (*SI Appendix*, Table S3).

PIE-FCCS measurements were collected on COS-7 cells expressing CXCR4-AcGFP1 and β2AR-mCherry. The median cross-correlation value was f_c = 0.02 (mean f_c = 0.02 ± 0.08, Fig. 4*B* and *SI Appendix*, Table S3), well below the f_c value for the 1×FPKB calibration standard (31). This suggests that there was no significant heterodimerization between the receptors in this cell line. PIE-FCCS measurements were then collected for DKO MDA-MB-231 cells expressing CXCR4-AcGFP1 and β2AR-mCherry, for which the cross-correlation values were significantly larger with a median f_c = 0.12 (f_c = 0.20 ± 0.22, Fig. 4*B* and *SI Appendix*, Table S3). Diffusion coefficient values also reflect the disparity in the degree of heteromerization in the different cellular contexts of COS-7 and MDA-MB-231. In COS-7 cells, the diffusion coefficients were similar to those in the homodimerization measurements for CXCR4 (0.22 ± 0.11 μm^2 s^{-1}) and β2AR (0.23 ± 0.19 μm^2 s^{-1}) (Fig. 4 *C* and *D* and *SI Appendix*, Table S3). In contrast, in DKO MDA-MB-231 cells, the average

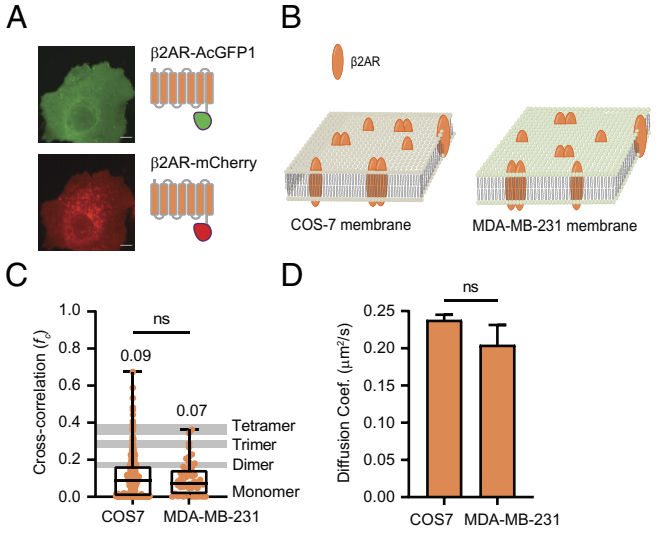

Fig. 3. Fractional correlation of β2AR shows weak homomultimerization in MDA-MB-231 and COS-7 cells. (*A*) Representative epifluorescence images of COS-7 cells expressing β2AR fused to AcGFP1 (*Top Left* image) and mCherry (*Bottom Left* image) at the C terminus and their schematic cartoons (*Right*). (Scale bars, 10 μm.) (*B*) Schematic showing the formation of β2AR homodimers in the COS-7 and MDA-MB-231 membranes. (*C*) Summary of single-cell cross-correlation values (f_c) for β2AR in COS-7 and MDA-MB-231 cells. The distribution of the f_c value of each individual cell was plotted, and the description of the plot is similar as in Fig. 1*E*. (*D*) Average diffusion coefficient of β2AR dimers in μm^2 of membrane area per second in COS-7 and MDA-MB-231 cells expressed as mean ± SD.

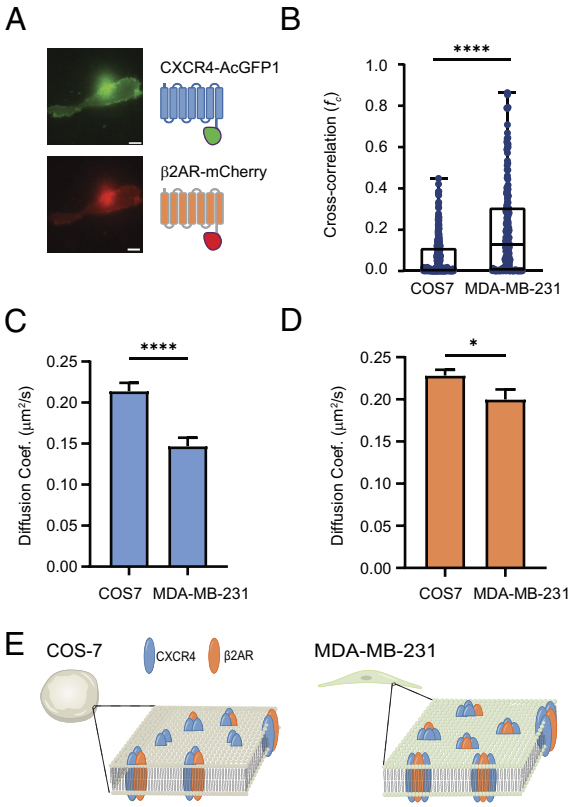

Fig. 4. β2AR associates with CXCR4 multimers in MDA-MB-231 cells. (*A*) Fluorescence image of CXCR4-AcGFP1 and β2AR-mCherry expressed in DKO MDA-MB-231 cells (scale bars are 10 μm). (*B*) Summary of single-cell cross-correlation values (f_c) for CXCR4 and β2AR heteromultimers in COS-7 and DKO MDA-MB-231 cells. The distribution of single-cell f_c values was plotted, and the description of the plot is similar as in Fig. 1*E*. (*C*) Average diffusion coefficient of CXCR4 in COS-7 and DKO MDA-MB-231 cells. (*D*) Average diffusion coefficient of β2AR dimers in COS-7 and DKO MDA-MB-231 cells. (*E*) Schematic showing the formation of CXCR4 and β2AR heteromultimers in COS-7 and DKO MDA-MB-231 cells.

diffusion coefficient of CXCR4 was 0.14 ± 0.13 $\mu m^2 s^{-1}$, consistent with the higher homomultimerization levels reported above. Interestingly, the diffusion coefficient of β2AR in the DKO MDA-MB-231 cells was slightly lower (0.19 ± 0.15 $\mu m^2 s^{-1}$) compared to the COS-7 cells (Fig. 4*D*), in contrast to the β2AR homodimerization measurements for which the diffusion coefficients were statistically indistinguishable. These results support the interpretation that β2AR associates with CXCR4 multimers in this cancer cell line. Similar measurements were performed in CHO and HCC4006 cells in which we saw significantly higher cross-correlation in human lung cancer cells (HCC4006) compared to CHO and COS-7 (*SI Appendix*, Fig. S3). Altogether, we interpret these results as β2AR monomers associating with CXCR4 multimers in the cancer cell lines as illustrated in Fig. 4*E*.

Ligand-Dependent Heterodimerization of CXCR4 and β2AR. Given the role of ligand binding in receptor behavior, we next examined whether CXCR4 and β2AR ligands would affect heteromultimerization between the two receptors. We coexpressed CXCR4-AcGFP1 and β2AR-mCherry in DKO MDA-MB-231 at similar levels as above and incubated the cells for 20 min with 0.1 μM CXCL12 or 5 μM epinephrine, the natural ligands of CXCR4 and β2AR, respectively (Fig. 5*A*). PIE-FCCS measurements were carried out in live cells before adding ligand and after the 20-min incubation time. The cells treated with CXCL12 showed no statistically significant change in their cross-correlation values with a median f_c = 0.12 (mean f_c = 0.12 ± 0.07) prior to treatment and a median f_c = 0.14 (mean f_c = 0.14 ± 0.08) after treatment (Fig. 5*B* and *SI Appendix*, Table S4). These results indicate that there was no significant change in the degree of heteromerization upon CXCL12 binding. The cells treated with epinephrine showed a substantial increase in the degree of cross-correlation with a median f_c = 0.19 compared to f_c = 0.12 in the untreated cells (Fig. 5*B*). These results suggest that epinephrine significantly increased the degree of multimerization between CXCR4 and β2AR in the DKO MDA-MB-231 cells. The combined administration of CXCL12 and epinephrine also enhances multimerization between CXCR4 and β2AR (Fig. 5*B*). Treatment with CXCR4 and β2AR antagonists, GPC-100 and propranolol, prior to adding CXCL12 and epinephrine abrogated the ligand-induced increase in multimerization (Fig. 5*B*). Independent of the degree of multimerization, the concomitant addition of ligands also induced visible puncta that were notably absent in the presence of the antagonists (*SI Appendix*, Fig. S5).

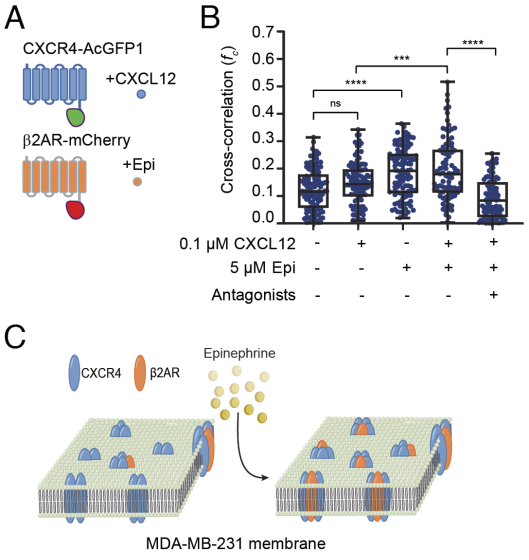

Fig. 5. CXCR4 and β2AR heteromultimerization is dependent on CXCL12 and epinephrine treatment in MDA-MB-231 cells. (*A*) Schematic of CXCR4 and β2AR fused to AcGFP1 and mCherry and their corresponding natural ligand. (*B*) Summary of single-cell cross-correlation values (f_c) for CXCR4 and β2AR heteromultimerization with (+) or without (−) ligand stimulation in the membranes of MDA-MB-231 cells. The distribution of f_c value of each individual cell was plotted, and the description of the plot is similar as in Fig. 1*E*. (*C*) Schematic showing the increased formation of CXCR4 and β2AR heteromultimers in MDA-MB-231 membranes after epinephrine treatment.

The diffusion coefficients for both CXCR4 and β2AR were only slightly reduced after addition of CXCL12 (*SI Appendix*, Table S3). Addition of epinephrine reduced the mobility of CXCR4 and β2AR by an even larger amount (about 30%), indicating a relative increase in multimerization compared to CXCL12 addition. When both CXCL12 and epinephrine were added, we observed a significant reduction of the diffusion coefficients (*SI Appendix*, Table S3). These results support the conclusion that CXCR4-β2AR interactions have a direct dependence on the ligand-binding state of β2AR.

The functional consequence of the CXCR4- β2AR heteromerization was observed as a synergistic effect on cell signaling when their respective ligands were added in combination to MDA-MB-231 cancer cells (*SI Appendix*, Fig. S6). Although the degree of heteromerization with the addition of epinephrine alone is similar to when both ligands are added, amplification of calcium flux and NFAT signaling occurred only when both ligands were present (*SI Appendix*, Fig. S6). The ligands also induce higher mRNA expression of IL-8 and PTGS2, whose overexpression has been found to be protumorigenic (*SI Appendix*, Fig. S7) (46–48). Addition of CXCR4 and β2AR antagonists reverse the effect of the ligands (*SI Appendix*, Fig. S7) as reported by our lab previously (49).

Discussion and Conclusions

Several GPCR heterodimers are currently under investigation for disease therapeutics (8, 9). However, no GPCR heteromer-targeting drug has been FDA approved. In this study, we applied a BiFC technology to perform an agnostic screen for GPCR heteromers in cancer cells. We then used a high information content method, PIE-FCCS, to validate and resolve the nature of these multimeric interactions for CXCR4 and β2AR. Although the role of CXCR4 in cancer is widely reported, it is intriguing to find that it interacts with β2AR, an important protein in stress response. In the results above, we observe that the addition of the β2AR ligand, epinephrine, alone can induce CXCR4 and β2AR heteromerization on the same scale as when both ligands are added. However, the synergistic effect of CXCR4 and β2AR dual targeting on signaling occurs only when both ligands are added. Along with our results on receptor antagonism, our data provide evidence that there is a complicated interplay between receptor structure, oligomerization, and signaling for GPCRs that has been previously underappreciated. A previous study has mapped out the residues and folded structures responsible for the different stages of CXCR4 Ca^{2+} flux upon CXCL12 binding (50). Our findings highlight the need to apply similar studies to heteromeric structures to fully resolve the atomic-scale structure and dynamics of GPCRs in different heteromultimeric states and the functional consequences of heteromerization.

PIE-FCCS measurements of these receptors at physiologically relevant densities of 10 to 2,000 molecules/μm^2 shed light on how different GPCRs can oligomerize on a live cell membrane. In the noncancer cell lines COS-7 and CHO cells, we find that CXCR4 exists as dimers on the membrane. This is consistent with a previous study wherein CXCR4 was identified to be in a monomer-dimer

equilibrium in CHO cells at densities ranging from <1 to ~100 molecules/μm^2 (4). Unexpectedly, we observed that CXCR4 assembles into multimeric complexes in the cancer cell lines MDA-MB-231 and HCC4006 cells. This suggests that different cellular environments can strongly affect the receptor oligomerization state. The extent to which this occurs is likely receptor-dependent, given that β2AR homodimerization did not differ in the different cellular contexts. The differential propensity of GPCRs to cluster in different cell lines suggests the need to determine whether the differences are attributable to lipid composition, the membrane protein milieu, or other cellular properties.

The PIE-FCCS results we reported here reveal a more complicated interaction scheme than a simple monomer-dimer equilibrium for CXCR4 and β2AR. Taking into consideration the observation of CXCR4 homomultimerization and weak β2AR homodimerization, we conclude that the heteromeric clusters are composed of one β2AR and several CXCR4 receptors. The interaction is weaker in the noncancer cell lines CHO and COS-7 cells, but significant in the cancer cell lines, MDA-MB-231 and HCC4006. We also report here that epinephrine increases the CXCR4- β2AR heteromerization. Correspondingly, it is possible that antagonizing this interaction could decrease the heteromerization and may have a therapeutic effect (51).

Materials and Methods

BiFC Assay. U-2 OS cells plated in 96-well plates are transduced with 30 MOI each of adenoviruses encoding CXCR4-VN and GPCRx-VC or CXCR4-VC and GPCRx-VN and incubated for 2 d to allow for protein expression. The plates were imaged with fluorescence microscopy to detect the nucleus with Hoechst 33342 and BiFC signal using an IN Cell Analyzer 1000. The fluorescence intensity per cell, as delineated by the Hoechst signal, was measured from the imagers. Cells with fluorescence intensities higher than the background level were considered BiFC-positive cells. Dead cells that showed extremely high intensities were excluded from the cell count. Positive cells were determined, and the positive cell count ratio ("BiFC score") was calculated as the number of positive cells divided by the total number of cells (100×).

Plasmid Construction. The fluorescent protein fusion constructs were generated by connecting AcGFP1 or mCherry to the C terminus of full-length human *CXCR4* (NCBI ID: AA36716.1) or human *ADRB2* (NCBI ID: NP_000015.2) with a serine/glycine-rich linker inserted in between. A Kozak consensus sequence was added by inserting ACC at position −3 and G at position +4 from the starting codon. CXCR4-AcGFP1, CXCR4-mCherry, ADRB2-AcGFP1, and ADRB2-mCherry constructs were synthesized (GenScript, USA; *SI Appendix*, Table S2) and subcloned into EcoRI/HindIII restriction sites in the multicloning site of pcDNA3.1(-) vectors (Invitrogen), and correct insertions were confirmed by Sanger sequencing. FKBP oligomer controls were based on the FK506-binding protein, as previously described (31), The constructs were transiently expressed in COS-7 cells after which the dimerizing agent (AP20187) was added, and after 20 min, PIE-FCCS were collected.

Generation of Stable CXCR4/ADRB2 Double Knockout Cell Lines. A group of ss-Oligos (*SI Appendix*, Table S3) was used to edit *CXCR4* and *ADRB2* genes in Wild-Type MDA-MB-231 cells. Specifically, asymmetrical single-stranded oligos were designed to introduce an in-frame premature stop codon and phosphorothioate modifications were included near the 5′ and 3′ ends of the oligos. Single-stranded DNA oligos CXCR4.1-sso and ADRB2.1-sso were designed against the sense strand to promote gene knockout (AAG > TAG) edit, CXCR4.2-sso and ADRB2.2-sso were designed against the antisense strand (TGG > TAG) edit, whereas CXCR4.3-sso and ADRB2.3-sso oligos were designed against the sense strand (TTC > TAG) edit. CRISPR IVT gRNAs were designed using GeneArt™ Precision gRNA Synthesis Kit and the DNA oligos were synthesized based on the gRNA designs. DNA oligos were amplified with PCR to generate DNA templates which were used in IVT reactions to synthesize gRNAs. The gRNAs were purified using MEGAclear™ Transcription Clean-Up Kit and had the following sequences: CXCR4.1 (GAAGCATGACGGACAAGTAC), CXCR4.2 (ACGGCATCAACTGCCCAGAA), CXCR4.3 (GTAGCGGTCCAGACTGATGA), ADRB2.1 (CAGACGCTCGAACTTGGCAA), ADRB2.2 (CGGTACCAGTGCATCTGAAT), ADRB2.3 (AAGAATATGGGCGGCCCCAA). These ss-Oligos were cotransfected with Cas9 nuclease and IVT gRNA (as RNP complex) in WT MDA-MB-231 to yield *CXCR4* and *ADRB2* gene knockouts For each electroporation, 1.5×10^5 cells were transfected with 250 ng of IVT gRNA, 1 μg of TrueCut™ Cas9 V2, and 1 μL of 10 μM ss-Oligo using the Neon® Transfection System with 1,400v/10 ms/4 pulses. 4× of each transfection was added to wells of a 6-well tissue culture plate already containing 2 mL of prewarmed DMEM (Dulbecco's modified Eagle medium). After 3 d posttransfection, cells were harvested and processed for Next Generation Sequencing to confirm KOs. To generate double knockout cells (DKOs), ADRB2.2 stable pool was transfected with CXCR4.2 IVT gRNA. Single growing colonies were scored using CloneSelect™ imager. The four selected clones were expanded, and QC tested with flow cytometry to measure the functional knockout of *CXCR4* and *ADRB2* genes (*SI Appendix*, Fig. S1).

Mammalian Cell Culture. WT MDA-MB-231 (ATCC HTB-26), COS-7 (ATCC CRL-1651), and HEK293 (Invitrogen) cells were maintained in DMEM (ATCC 30-2002) supplemented with 10% FBS (Gibco), 1% L-glutamine (Corning), and 1% penicillin/streptomycin (Corning) and incubated at 37 °C in 5% CO2. U-937 (Korean Cell Line Bank 21593.1) and MM.1S (ATCC CRL-2974) cells were maintained in RPMI (Gibco), and U-2 OS cells (ATCC HTB-96) were maintained in McCoy's 5A medium supplemented with 10% FBS (Gibco) and 1% penicillin/streptomycin (Gibco).

Sample Preparation for PIE-FCCS. MDA-MB-231 (WT and DKO) and COS-7 cells were dissociated, resuspended in DMEM, and reseeded at 0.3×10^6 cells in 35 mm MatTek plates for transfection. Lipofectamine 2000 (Invitrogen) and lipofectamine 3000 (Invitrogen) were used to transfect COS-7 and MDA-MB-231, respectively. PIE-FCCS measurements were taken after 24 h of transfection.

PIE-FCCS Instrument Setup and Alignment. PIE-FCCS measurements were performed as previously described (34). Briefly, the custom-built Nikon confocal microscope (Eclipse Ti, Nikon Instruments) uses a 50 ns pulsed continuum white laser source (SuperK Extreme, NKT Photonics) that goes through a beam splitter (Spectrak Split, NKT Photonics) to split the beam into two wavelengths, 488 nm and 561 nm. These two lasers are directed through individual optical fibers of 15 m difference in length to induce a delay in arrival time relative to each other allowing for the pulsed interleaved excitation and the elimination of spectral cross talk between the detectors. The two lasers were aligned before entering the microscope through a dichroic beam splitter (LM01-503-25, Semrock) and a filter cube (zt488/561rpc, zet488/561 m, Chroma Technology). A 100× TIRF oil objective (Nikon) was used for the excitation laser focus and emitted fluorescence collection. The two excitation beams were microadjusted to ensure that they both illuminate the same spot of the flat, peripheral membrane area of the cell where the space between the apical and basal membranes is within a few hundred nanometers. Thus, providing a dual color excitation of AcGFP1 and mCherry-tagged receptors in the excited membrane area and avoiding the inclusion of fluorescence from cytosolic fluorescent proteins. A short fluorescently tagged DNA oligonucleotide (41 base pairs), with a TAMARA dye on the 5′ end and a 6-FAM dye on the 3′ end, was used to verify the alignment of the system, including the confocal volume overlap. Laser powers were set to 400 nW for 488 nm beam and 700 nW for 561 nm beam using an energy meter (Thorlabs). The two beams were overlapped and focused to the back of the microscope and through the objective to a diffraction-limited spot on a peripheral membrane area of the cell. The respective green and red emitted photons were detected using a home-built confocal detection unit with a 50 μm confocal pinhole and dichroic beam splitter (LM01-503-25, Semrock). The two signals were bandpass filtered (91032, Chroma Technology Corp.) and then separately focused on to single-photon avalanche photodiodes (Micro Photon Devices). The signals were recorded using two channel time-correlated single-photon counting modules (PicoHarp 300, PicoQuant).

PIE-FCCS Data Collection and Analysis. Samples (COS-7, CHO, and MDA-MB-231 cells) on MatTek plates were placed on the stage housed in a 37 °C stage incubator. The cells were observed using epifluorescence mode for AcGFP1 and mCherry channels. For each single cell selected for measurement, the 488 nm and 561 nm lasers were focused on the peripheral of the cell, and the time-tagged time-resolved data (TTTR) were collected using PicoHarp 300 software. A total of six

acquisitions were collected on one spot for 10 s each. Data were binned at 100 ms. Time gating for channel A (red) was set at 2,350 and 3,100 as the lower and upper bounds and was set at 1 and 600 as the lower and upper bounds for channel B (green). A (red autocorrelation), B (green autocorrelation), and X (cross-correlation) functions were then applied to data, generating curves for each individual acquisition, for a total of six sets of curves for each cell and are described below.

$$G_i(\tau) = \frac{\langle \delta F_i(t) \cdot \delta F_i(t+\tau) \rangle}{\langle \delta F_i(t) \rangle^2}. \quad [\mathbf{1}]$$

Autocorrelation function applied for fluorescence signal in green and red channels, $\delta F_i(t)$ represents fluctuations in fluorescence. These fluctuations are correlated to a lag time τ Angled brackets represent binned data. This equation is then expanded to generate the cross-correlation curve as shown in Eq. **2**

$$G_X(\tau) = \frac{\langle \delta F_R(t) \cdot \delta F_G(t+\tau) \rangle}{\langle \delta F_R(t) \rangle \cdot \langle \delta F_G(t) \rangle}. \quad [\mathbf{2}]$$

Individual curves were then averaged and fitted to a two-dimensional diffusion model with triplet-blinking using a nonlinear least squares model as shown in Eq. **3**.

$$G(\tau) = G(0)\frac{\left(1 - F - Fe^{-\tau/-\tau}T\right)}{(1-F)}\frac{1}{\left(1+\frac{\tau}{\tau_D}\right)}, \quad [\mathbf{3}]$$

where F is the triplet state fraction, τ_t is the triple state lag time, τ_D is the dwell time, and $G(0)$ is the correlation function amplitude that is inverse to the average diffusing species population.

After correlation curves have been fit, initial correlation function amplitudes are used to calculate the fraction of correlated proteins (f_c) as shown blow.

$$f_c = \frac{G_x(0)}{\max\left(G_G(0), G_R(0)\right)}, \quad [\mathbf{4}]$$

where $G_G(0)$, $G_R(0)$, and $G_x(0)$represent the initial correlation function values for green autocorrelation functions, red autocorrelation functions, and cross-correlation functions, respectively.

Flow Cytometry. MDA-MB-231 (WT and DKO) and COS-7 cells either endogenous or transiently transfected with CXCR4-AcGFP1, CXCR4-mCherry, β2AR-AcGFP1, or β2AR-mCherry were seeded at 5×10^5 cells/well in six-well plates until they reached confluency. Cells were then washed once with 1× PBS, incubated with cell dissociation buffer (Accutase, Invitrogen, 00-4555-56) for 2 min at 37 °C, and then washed thrice with ice-cold PBS with 2% FBS. Cells were incubated in the dark for 30 min with gentle rotation in ice-cold PBS (with 2% FBS) containing the following conjugated-primary antibodies: APC anti-human CXCR4 (BioLegend, 306510), Alexa488 anti-β_2-AR (R&D Systems 586107), and isotype controls APC anti-mouse IgG2a, κ (BioLegend, 400222), Alexa488 normal mouse IgG_1 (Santa Cruz, sc-3890). Cells were then washed three times and suspended in ice-cold PBS containing 2% FBS for final flow cytometric analysis. Flow cytometry was performed using BD Accuri C6 Plus flow cytometer (BD Biosciences) and BD Accuri C6 Plus software (1/2016) for data acquisition. Alexa Flour 488 was excited using a 488 nm laser, filtered through 533/30 nm, and detected with FL1. APC was excited using a 640 nm laser, filtered through 675/25 nm, and detected with FL4. Gating for background was determined using unlabeled cells. Data analysis was performed using FlowJo software (v10.8; Becton, Dickinson, & Co.).

Calcium Flux Assay. MDA-MB-231 cells, stably expressing CXCR4 and β2AR through lentiviral transduction, were plated at 4×10^4 cells/well in a 96-well black clear-bottom microplate. The following day, cells were stained with Cal-520 AM (AAT Bioquest) for 2 h at 37 °C, and intracellular calcium mobilization was measured using a Flexstation 3 microplate reader (Molecular Devices).

NFAT-Luciferase Reporter Assay. MDA-MB-231 cells, stably expressing CXCR4 and β2AR through lentiviral transduction, were plated at 2×10^4 cells/well in a 96-well white-bottom plate and transduced with adenoviruses encoding NFAT-RE-*luc2P* reporter (Promega). After incubation for 2 d, the cells were treated with agonists for 6 h at 37 °C. Luciferase activity was quantified using Steady-Glo reagent (Promega) with Varioskan LUX microplate reader (Thermo Fisher Scientific).

IL-8 and PTGS2 qRT-PCR. MDA-MB-231 cells were culture in serum starved overnight (16 h) and applied to pretreatment with 10 μM of AMD3100 (anti-CXCR4) and ICI-118,551 (anti- β2AR) as indicated before treatment of CXCL12 and epinephrine respectively. After 6 h incubation of CXCL12 and epinephrine, the cells were harvested, and mRNA levels of IL-8 and PTGS2(COX2) were detected by qRT-PCR. The values were normalized to β-actin mRNA levels. The error bars represent the means ± SD from three independent experiments.

Statistical Analysis. All data presented in figures and *SI Appendix*, Figs. S1–S7 are mean ± SEM of at least three independent experiments unless stated differently in the figure legends. PIE-FCCS data were analyzed using MATLAB (MathWorks) and Excel spreadsheet. Fluorescent images were analyzed using ImageJ (NIH). Statistical analyses were performed using GraphPad Prism (GraphPad Software). *P*-values were determined using the paired *t* test where $^{****}P < 0.01$ is highly significant, $^{*}P < 0.05$ is significant, and ns is not significant.

Data, Materials, and Software Availability. Previously published data were used for this work (The data in Fig. 2*G* were previously published in ref. 31). All other data are included in the manuscript and/or *SI Appendix*.

ACKNOWLEDGMENTS. This work was supported by the Human Frontiers of Science Program (RGP0059/2019), GPCR Therapeutics Inc., and the National Research Foundation of Korea (2020R1A5A1018081). GPCR Therapeutics Inc. sponsored the research preformed at the University of Akron and Texas Tech University.

Author affiliations: [a]Department of Chemistry, University of Akron, Akron, OH 44325; [b]Department of Chemistry and Biochemistry, Texas Tech University, Lubbock, TX 79409; [c]GPCR Therapeutics Inc., Gwanak-gu, Seoul 08790, Republic of Korea; [d]School of Biological Sciences, Seoul National University, Seoul 08826, Republic of Korea; and [e]Institute of Microbiology, Seoul National University, Seoul 08826, Republic of Korea

1. K. Sriram, P. A. Insel, G protein-coupled receptors as targets for approved drugs: How many targets and how many drugs? *Mol. Pharmacol.* **93**, 251–258 (2018).
2. S. Ferré, F. Ciruela, V. Casadó, L. Pardo, Oligomerization of G protein-coupled receptors: Still doubted? *Prog. Mol. Biol. Transl. Sci.* **169**, 297–321 (2020).
3. S. Ferré *et al.*, Building a new conceptual framework for receptor heteromers. *Nat. Chem. Biol.* **5**, 131–134 (2009).
4. A. Işbilir *et al.*, Advanced fluorescence microscopy reveals disruption of dynamic CXCR4 dimerization by subpocket-specific inverse agonists. *Proc. Natl. Acad. Sci. U.S.A.* **117**, 29144–29154 (2020).
5. J. A. Burger, A. Peled, CXCR4 antagonists: Targeting the microenvironment in leukemia and other cancers. *Leukemia* **23**, 43–52 (2009).
6. B. Debnath, S. Xu, F. Grande, A. Garofalo, N. Neamati, Small molecule inhibitors of CXCR4. *Theranostics* **3**, 47–75 (2013).
7. D. D. Mushtaq Ahmad Nengroo, M. Ali Khan, A. Verma, Demystifying the CXCR4 conundrum in cancer biology: Beyond the surface signaling paradigm. *Biochim. Biophys. Acta - Rev. Cancer* **1877**, 188790 (2022).
8. S. Taromi *et al.*, CXCR4 antagonists suppress small cell lung cancer progression. *Oncotarget* **7**, 85185–85195 (2016).
9. L. Qiu, Y. Xu, H. Xu, B. Yu, The clinicopathological and prognostic value of CXCR4 expression in patients with lung cancer: A meta-analysis. *BMC Cancer* **22**, 1–13 (2022).
10. C. Lapa *et al.*, Oncotarget 9288. www.impactjournals.com/oncotarget [68 Ga]Pentixafor-PET/CT for imaging of chemokine receptor 4 expression in small cell lung cancer-initial experience. *Oncotarget* **7**, 9288–9295 (2016).
11. Y. Percherancier *et al.*, Bioluminescence resonance energy transfer reveals ligand-induced conformational changes in CXCR4 homo- and heterodimers. *J. Biol. Chem.* **280**, 9895–9903 (2005).
12. B. Wu *et al.*, Structures of the CXCR4 chemokine GPCR with small-molecule and cyclic peptide antagonists. *Science* **330**, 1066–1071 (2010).
13. S. Armando *et al.*, The chemokine CXC4 and CC2 receptors form homo- and heterooligomers that can engage their signaling G-protein effectors and βarrestin. *FASEB J.* **28**, 4509–4523 (2014).
14. B. Ge *et al.*, Single-molecule imaging reveals dimerization/oligomerization of CXCR4 on plasma membrane closely related to its function. *Sci. Rep.* **7**, 1–9 (2017).
15. J. S. Paradis *et al.*, Computationally designed GPCR quaternary structures bias signaling pathway activation. *Nat. Commun.* **13**, 1–14 (2022).

16. M. Hamatake *et al.*, Ligand-independent higher-order multimerization of CXCR4 a G-protein-coupled chemokine receptor involved in targeted metastsasis. *Cancer Sci.* **100**, 95–102 (2009).
17. L. Martínez-Muñoz *et al.*, Separating actin-dependent chemokine receptor nanoclustering from dimerization indicates a role for clustering in CXCR4 signaling and function. *Mol. Cell* **70**, 106–119. e10 (2018).
18. N. Isik, D. Hereld, T. Jin, Fluorescence resonance energy transfer imaging reveals that chemokine-binding modulates heterodimers of CXCR4 and CCR5 receptors. *PLoS One* **3**, e3424 (2008).
19. M. M. Hammad, Y. Q. Kuang, R. Yan, H. Allen, D. J. Dupre, Na+/H+ exchanger regulatory factor-1 is involved in chemokine receptor homodimer CCR5 internalization and signal transduction but does not affect CXCR4 homodimer or CXCR4–CCR5 heterodimer. *J. Biol. Chem.* **285**, 34653–34664 (2010).
20. A. O. Watts *et al.*, Identification and profiling of CXCR3-CXCR4 chemokine receptor heteromer complexes. *Br. J. Pharmacol.* **168**, 1662–1674 (2013).
21. F. M. Décaillot *et al.*, CXCR7/CXCR4 heterodimer constitutively recruits β-arrestin to enhance cell migration. *J. Biol. Chem.* **286**, 32188–32197 (2011).
22. C. J. Coke *et al.*, Simultaneous activation of induced heterodimerization between CXCR4 chemokine receptor and cannabinoid receptor 2 (CB2) reveals a mechanism for regulation of tumor progression. *J. Biol. Chem.* **291**, 9991–10005 (2016).
23. X. Chen *et al.*, Biased activation mechanism induced by GPCR heterodimerization: Observations from μoR/δOR dimers. *J. Chem. Inf. Model.* **62**, 5581–5600 (2022).
24. J. Liu *et al.*, Biased signaling due to oligomerization of the G protein-coupled platelet-activating factor receptor. *Nat. Commun.* **13**, 6365 (2022).
25. M. R. Stoneman *et al.*, A general method to quantify ligand-driven oligomerization from fluorescence-based images. *Nat. Methods* **16**, 493–496 (2019).
26. P. Annibale, M. J. Lohse, Spatial heterogeneity in molecular brightness. *Nat. Methods* **17**, 273–275 (2020).
27. K. Bacia, S. A. Kim, P. Schwille, Fluorescence cross-correlation spectroscopy in living cells. *Nat. Methods* **3**, 83–89 (2006).
28. B. K. Müller, E. Zaychikov, C. Bräuchle, D. C. Lamb, Pulsed interleaved excitation. *Biophys. J.* **89**, 3508–3522 (2005).
29. N. F. Endres *et al.*, Conformational coupling across the plasma membrane in activation of the EGF receptor. *Cell* **152**, 543–556 (2013).
30. Y. Huang *et al.*, Molecular basis for multimerization in the activation of the epidermal growth factor receptor. *Elife* **5**, 1–27 (2016).
31. M. J. Kaliszewski *et al.*, Quantifying membrane protein oligomerization with fluorescence cross-correlation spectroscopy. *Methods* **140–141**, 40–51 (2018).
32. W. B. Asher *et al.*, Single-molecule FRET imaging of GPCR dimers in living cells. *Nat. Methods* **18**, 397–405 (2021).
33. S. M. Christie *et al.*, Covalently immobilizing interferon-γDrives filopodia production through specific receptor-ligand interactions independently of canonical downstream signaling. *Bioconjug. Chem.* **31**, 1362–1369 (2020).
34. W. D. Comar, S. M. Schubert, B. Jastrzebska, K. Palczewski, A. W. Smith, Time-resolved fluorescence spectroscopy measures clustering and mobility of a G protein-coupled receptor opsin in live cell membranes. *J. Am. Chem. Soc.* **136**, 8342–8349 (2014).
35. T. H. Lan *et al.*, BRET evidence that β2 adrenergic receptors do not oligomerize in cells. *Sci. Rep.* **5**, 1–12 (2015).
36. M. Pérez-Sayáns *et al.*, β-adrenergic receptors in cancer: Therapeutic implications. *Oncol. Res.* **19**, 45–54 (2010).
37. K. S. R. Sastry *et al.*, Epinephrine protects cancer cells from apoptosis via activation of cAMP-dependent protein kinase and BAD phosphorylation. *J. Biol. Chem.* **282**, 14094–14100 (2007).
38. M. Gruet *et al.*, β2-adrenergic signalling promotes cell migration by upregulating expression of the metastasis-associated molecule LYPD3. *Biology (Basel).* **9**, 1–25 (2020).
39. C. Pérez Piñero, A. Bruzzone, M. G. Sarappa, L. F. Castillo, I. A. Lüthy, Involvement of α2- and β2-adrenoceptors on breast cancer cell proliferation and tumour growth regulation. *Br. J. Pharmacol.* **166**, 721–736 (2012).
40. S. Angers *et al.*, Detection of β 2 -adrenergic receptor dimerization in living cells using bioluminescence resonance energy transfer (BRET). *Proc. Natl. Acad. Sci. U.S.A.* **97**, 3684–3689 (2000).
41. T. J. Larocca *et al.*, β2-adrenergic receptor signaling in the cardiac myocyte is modulated by interactions with CXCR4. *J. Cardiovasc. Pharmacol.* **56**, 548–559 (2010).
42. D. Calebiro *et al.*, Single-molecule analysis of fluorescently labeled G-protein-coupled receptors reveals complexes with distinct dynamics and organization. *Proc. Natl. Acad. Sci. U.S.A.* **110**, 743–748 (2013).
43. Y. B. Song, C. O. Park, J. Y. Jeong, W. K. Huh, Monitoring G protein-coupled receptor activation using an adenovirus-based β-arrestin bimolecular fluorescence complementation assay. *Anal. Biochem.* **449**, 32–41 (2014).
44. C. D. Hu, Y. Chinenov, T. K. Kerppola, Visualization of interactions among bZIP and Rel family proteins in living cells using bimolecular fluorescence complementation. *Mol. Cell* **9**, 789–798 (2002).
45. C. Park *et al.*, Simultaneous activation of CXC chemokine receptor 4 and histamine receptor H1 enhances calcium signaling and cancer cell migration. *Sci. Rep.* **13**, 1–13 (2023).
46. K. Fousek, L. A. Horn, C. Palena, Interleukin-8: A chemokine at the intersection of cancer plasticity, angiogenesis, and immune suppression. *Pharmacol. Ther.* **219**, 1–16 (2021).
47. X. M. Lin *et al.*, The role of prostaglandin-endoperoxide synthase-2 in chemoresistance of non-small cell lung cancer. *Front. Pharmacol.* **10**, 1–14 (2019).
48. M. V. Kamal, R. R. Damerla, P. S. Dikhit, N. A. Kumar, Prostaglandin-endoperoxide synthase 2 (PTGS2) gene expression and its association with genes regulating the VEGF signaling pathway in head and neck squamous cell carcinoma. *J. Oral Biol. Craniofacial Res.* **13**, 567–574 (2023).
49. D. D. Sukhtankar *et al.*, GPC-100, a novel CXCR4 antagonist, improves in vivo hematopoietic cell mobilization when combined with propranolol. *PLoS One* **18**, 1–23 (2023).
50. M. P. Wescott *et al.*, Signal transmission through the CXC chemokine receptor 4 (CXCR4) transmembrane helices. *Proc. Natl. Acad. Sci. U.S.A.* **113**, 9928–9933 (2016).
51. L. Liu *et al.*, Allosteric ligands control the activation of a class C GPCR heterodimer by acting at the transmembrane interface. *Elife* **10**, 1–22 (2021).